Hindawi
Shock and Vibration
Volume 2019, Article ID 3526727, 10 pages
https://doi.org/10.1155/2019/3526727

Research Article

Effects of Strain Rate and Initial Density on the Dynamic Mechanical Behaviour of Dry Calcareous Sand

Zhangyong Zhao,[1] **Yanyu Qiu**,[1,2] **and Mingyang Wang**[1,2]

[1]*State Key Laboratory of Disaster Prevention and Mitigation of Explosion and Impact, The Army Engineering University of PLA, Nanjing, Jiangsu 210007, China*
[2]*School of Mechanical Engineering, Nanjing University of Science and Technology, Nanjing, Jiangsu 210094, China*

Correspondence should be addressed to Zhangyong Zhao; zhaozhangyong1@126.com

Received 15 May 2019; Accepted 8 July 2019; Published 22 July 2019

Academic Editor: Giuseppe Ruta

The dynamic compressive behaviour of dry calcareous sand under rigid confinement was characterised using a split-Hopkinson pressure bar (SHPB). Sand samples were confined inside a sleeve of hardened stainless steel and capped by a pair of aluminium cylindrical rods. This assembly was subjected to repeated dynamic compaction to attain precise bulk mass densities. It was then sandwiched between the incident and transmission bars of SHPB for dynamic compression testing. Sand specimens of three initial mass densities, namely, 1.26 g/cm^3, 1.35 g/cm^3, and 1.42 g/cm^3, were loaded by incident pulses applying a stress of 35 MPa, 71 MPa, and 143 MPa, respectively. Experimental results show that in the strain rate range of 335 s^{-1} to 1253 s^{-1}, the dynamic mechanical behaviours of dry calcareous sands exhibited no significant strain rate effect. The Lundborg model and the Murnaghan model could be used to describe the deviatoric and volumetric behaviours of calcareous sand with different initial densities, respectively.

1. Introduction

Calcareous sand is generally regarded as an oceanic sediment which contains an appreciable amount (>30%) of $CaCO_3$, leading to certain mechanical properties compared with continental sediments such as quartz sand [1, 2]. It usually originates from reworked shell fragments and skeletal debris of marine organisms and is widely distributed on coral reefs and seashores throughout the world such as in the South China Sea, Red Sea, west continental platform of Australia, and the Bass Strait [3, 4]. With the rapid development of the offshore construction, the mechanical response of calcareous sand has attracted the attention of engineers. Generally, it is found that calcareous sand includes large amounts of irregular crushable particles, leading to a higher compressibility and more significant grain crushing at elevated stresses than continental sediments [5–8]; however, compared with extensive studies under quasistatic condition, few studies consider the dynamic compressive behaviour of calcareous sand, which is important in some special engineering problems such as dynamic compaction and mine blast situations, and in air-raid shelters.

Farr used a uniaxial strain device (WES 0.1 msec) to study the effect of loading rate on the one-dimensional compressibility of dense partially saturated Enewetak calcareous sand [9]. The test results show that when the strain rate of calcareous sand sample increases from 10^{-3} s^{-1} to 300 s^{-1}, the constrained modulus can be increased by 120%. In recent years, the split-Hopkinson pressure bar (SHPB) has been widely used to study the dynamic mechanical behaviour of sand [10–12]. Bragov computed the lateral stress component of the specimen based on measurements of circumferential strain, which, together with obtaining the longitudinal stresses in the specimen using the SHPB method, make it possible to find the deviatoric stress and the hydrostatic pore water pressure in the specimen; however, in most studies, using this method, the soil under test is a quartz sand [13–18]. No experimental research has yet been

aimed at the study of the deviatoric and volumetric behaviour of calcareous sand. Lv et al. studied the one-dimensional dynamic compressive behaviour of dry calcareous sand and dry silica sand with the same relative density and similar strain rate using the SHPB method [19], and the experimental results show that the apparent modulus of calcareous sand under dynamic loading is approximately 10% of that of silica sand; however, the effects of strain rate and initial density of the sample on the dynamic mechanical behaviour of dry calcareous sand under stiff confinement were not investigated in their studies. These effects will be studied by using the SHPB method in the present research, and the deviatoric and volumetric behaviours will be analysed based on the experimental results.

2. Experimental Work

2.1. Sand Samples. The white calcareous sand used in this research is from the South China Sea. The micrographs of calcareous sands obtained by using the Hitachi S-4800 scanning electron microscope are shown in Figure 1, which shows that the sand particles are mostly angular with many interparticle voids in the calcareous sand particles, leading to its complex microstructure and the low strength of the particles.

All the sand samples used in this research were first oven-dried. The grain size distribution curve of the sample is shown in Figure 2, which was determined by using the laser-diffractometry instrument called Mastersizer 3000E. According to the result, the average particle size and the uniformity coefficient of the calcareous sand are 0.348 mm and 8.84, respectively. The particle density of sand particle was determined to be 2.81 g/cm^3. The minimum and maximum dry density of the sand is 1.12 g/cm^3 and 1.47 g/cm^3; these properties were tested based on ASTM methods [19–22].

To study the effect of the initial mass density of the sample on the dynamic mechanical behaviour of calcareous sand, three types of samples with initial dry density of 1.42 g/cm^3, 1.35 g/cm^3, and 1.26 g/cm^3 were designed. The relative densities of these samples are 89%, 72%, and 47%, respectively.

2.2. Experimental Setup. Dynamic experiments are carried out with a standard split-Hopkinson pressure bar apparatus (Figure 3), including a set of solid bars and a strain data acquisition system. The striker, the incident bar, and the transmission bar are made of aluminium alloy with a diameter of 37 mm and lengths of 600 mm, 2000 mm, and 2000 mm, respectively. The density, Young's modulus, Poisson's ratio, and bar wave speed of the aluminium material used are 2.8 g/cm^3, 73 GPa, 0.324, and 5107 m/s, respectively. As its impedance is lower than that of steel, the aluminium material is suitable for the SHPB tests associated with low-impedance soil. The sand samples were loaded by the striker and the incident bar, and their dynamic strain and stress during loading were obtained by calculating the stress wave velocity in the incident bar and transmission bar based on elastic wave theory [23].

To study the strain rate effect on the dynamic mechanical behaviour of calcareous sand, the sand samples were loaded by the striker with three nominal velocities, namely, 5 m/s, 10 m/s, and 20 m/s. Based on the elastic wave theory [24], the corresponding nominal stresses applied via the incident impulse are 35 MPa, 71 MPa, and 143 MPa, respectively. The actual velocity of the striker was measured by using a laser velocimeter with 0.1 m/s resolution.

The sample container consists of a sleeve, a pair of sealing rods, and a pair of locating rods. The sleeve was made of stainless steel and was designed to provide rigid confinement for the samples. The inner diameter, the outer diameter, and height of the sleeve are 37.05 mm, 47.05 mm, and 90 mm, respectively. The sealing rods together with the locating rods were used to locate and control the initial height and density of the sample. They were made of the same aluminium alloy as the pressure bar with a diameter of 37 mm and length of 20 mm. The sealing rod has a sealing groove with a width of 4.2 mm and a depth of 5 mm for mounting the Glyd Ring, which was used to fix the sealing rod in the sleeve during sample preparation and prevent the loss of sand particles during loading.

Figure 4 schematically shows the sample height and its position in the container. As is shown, the initial height of the sand sample is 10 mm, so the initial volume of the sample is 10.75 cm^3. The mass of the sample that is needed to fill the container could be calculated through multiplying its initial density and volume. To prepare a sample with a given density, a locating rod and a sealing rod were firstly put into the vertically placed sleeve. Then, the sample with the corresponding mass was poured into the container, and another sealing rod and locating rod were placed in the container. A 1.25 kg hammer was continuously dropped from a height of 300 mm to strike the top surface of the locating rod until it was flushed with the top surface of the sleeve. Finally, two locating rods were taken out of the container, and a bolt was screwed into the hole in the top sealing rod to prevent the loss of sand particles under loading. The container, together with the sand sample, could then be sandwiched between the incident bar and the transmission bar (Figure 3).

A strain gauge was attached to the external surface of the sleeve to measure the circumferential strain of the sleeve, and the strain will be used to calculate the lateral stress on the specimen based on elastic mechanics [25].

For the sands tested here, the sample diameter is the same as the bar diameter; when the sample is in a state of uniform stress, the strain and stress histories of the sample could be calculated as [14]

$$\dot{\varepsilon}(t) = \frac{C_0}{L_s}\left[\varepsilon_i(t) - \varepsilon_r(t) - \varepsilon_t(t)\right],$$

$$\varepsilon(t) = \frac{C_0}{L_s}\int_0^t \left[\varepsilon_i(t) - \varepsilon_r(t) - \varepsilon_t(t)\right]dt, \quad (1)$$

$$\sigma(t) = \frac{E_0}{2}\left[\varepsilon_i(t) + \varepsilon_r(t) + \varepsilon_t(t)\right],$$

where $\varepsilon_i(t)$, $\varepsilon_r(t)$, and $\varepsilon_t(t)$ are incident, reflected, and transmitted strain histories measured by using the axial strain gauges on the solid bars, respectively; E_0 and C_0 are

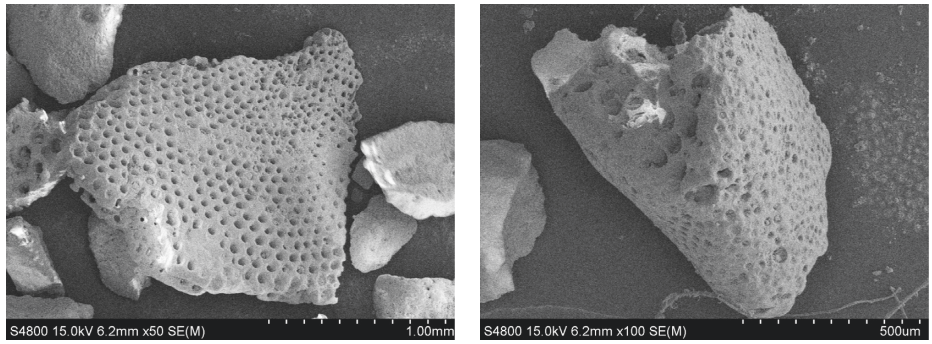

(a) (b)

Figure 1: SEM micrographs of the calcareous sands. (a) 50x magnification. (b) 100x magnification.

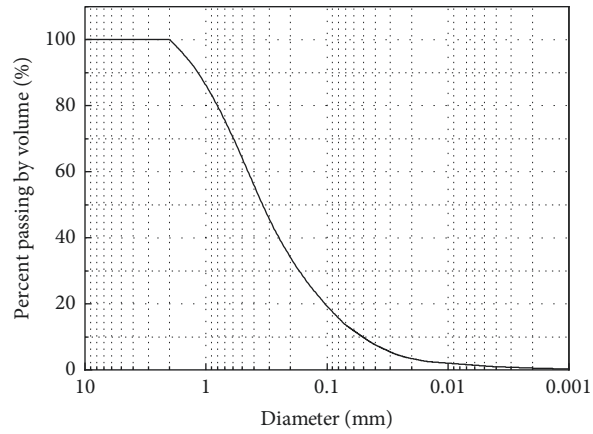

Figure 2: Particle size distribution curve of both sands.

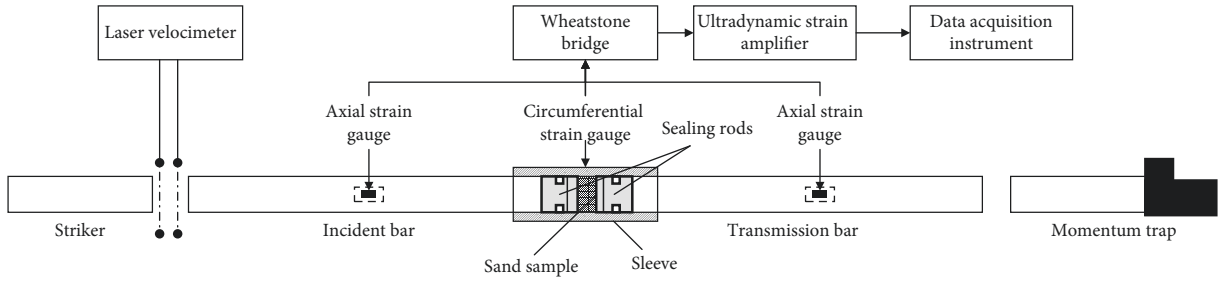

Figure 3: Schematic of the SHPB apparatus used for dynamic compaction of sand.

Young's modulus and elastic wave speed of the bar material, respectively; L_s is the initial length of the specimen. Therefore, once the incident, reflected, and transmitted signals are measured, the axial strain-stress data for the sand under investigation can be obtained by eliminating the time variable of the strain and stress histories of the sample.

3. Experimental Results

3.1. Axial Strain-Stress Relationship of Dry Calcareous Sand. In this research, three independent replicates were performed for each test group with different sample densities and striker velocities, and the corresponding basic results are summarised in Table 1.

Figure 5 shows a typical set of strain records of calcareous sand in test group CS9. It could be found that the rise time of the incident pulse is very short, so the dispersive effects of the pulses need to be corrected. In this research, Bussac's and Tyas's correction methods were used to correct for dispersive effects [26–28]. After correction, the strain records could be used to calculate the strain and stress histories of the sample based on equation (1).

Dynamic stress equilibrium was checked by the "2-wave," "1-wave" method as used by Song [14] (Figure 6). The stress history of sample front end was calculated by adding the

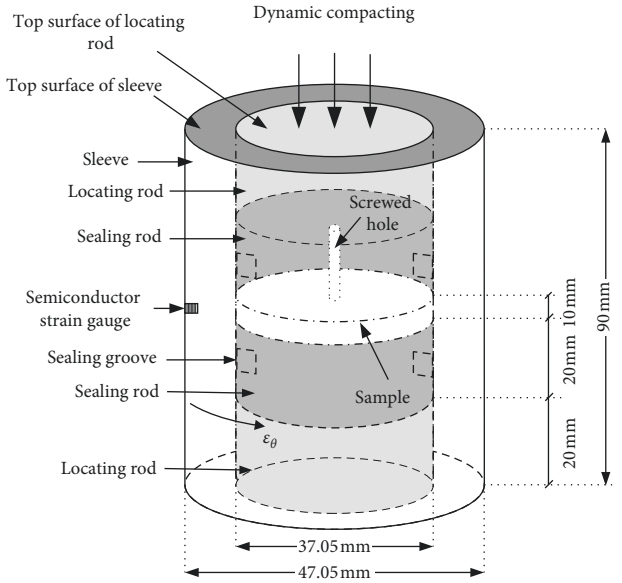

Figure 4: Schematic diagram of the sample in the container.

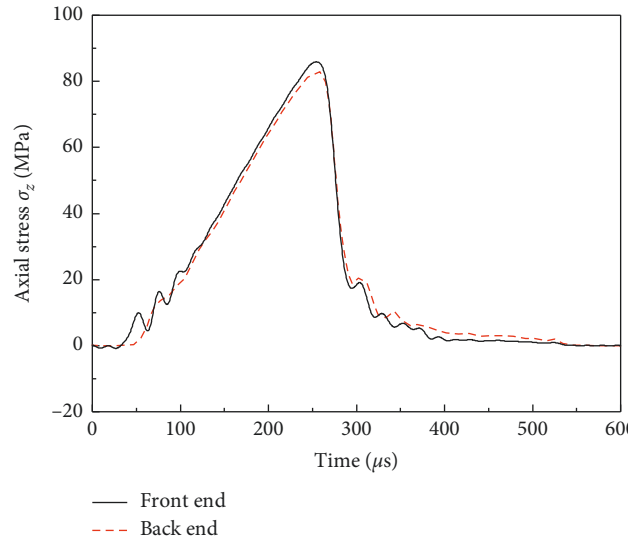

Figure 6: Dynamic stress equilibrium in the sand sample (test group number: CS9).

Table 1: Experimental results of calcareous sand.

Test group number	Initial sample density (g/cm^3)	Average striker velocity (m/s)	Average sample strain rate (s^{-1})	Average sample peak strain	Average sample peak stress (MPa)
CS1	1.26	5.3	385	0.104	6.4
CS2		10.5	748	0.192	18.5
CS3		19.2	1253	0.314	61.5
CS4	1.35	5.1	412	0.097	10.2
CS5		9.6	693	0.177	24.7
CS6		19.9	1189	0.293	77.1
CS7	1.42	4.0	335	0.080	12.5
CS8		9.8	487	0.118	17.8
CS9		21.4	1128	0.273	90.8

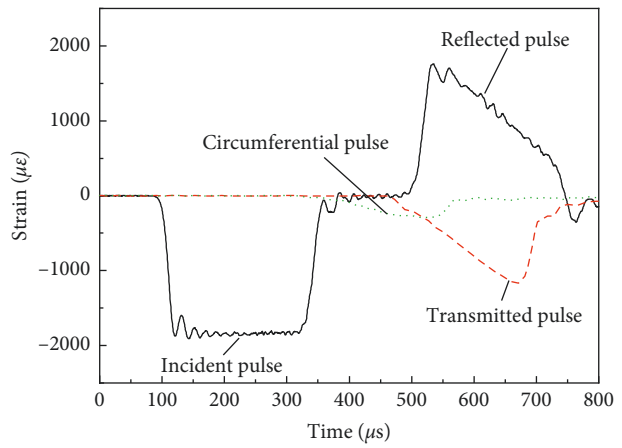

Figure 5: Typical set of strain records of calcareous sand (test group number: CS9).

incident stress wave to the reflected stress wave, while the stress history of sample back end equals the transmitted stress wave. It can be seen from the figure that the stress histories at both ends of the sample almost overlapped except during the initial stage of loading, indicating that the stress in the specimen was uniform under most load conditions.

After the dynamic stress equilibrium is satisfied in the sample, the strain-stress curve of the experiment calculated by equation (1) is valid. Following the similar procedure, the mean curves with error bars for samples of the same initial density are plotted (Figures 7(a)–7(c)). There are oscillations in the stress-strain curves at small strains. By comparing the stress from the stress-strain curves and the corresponding stress histories at both ends of the sample (Figure 6), it was concluded that the oscillations were caused by out-of-equilibrium stresses in the sand sample. Despite the stress nonequilibrium at the initial deformation stage, the results showed no significant differences under overlapping stress ranges with different strain rates, indicating that, in the strain rate range of 335 s^{-1} to 1253 s^{-1}, the dynamic compression characteristics of dry calcareous sand exhibited no significant rate effect.

After discarding the nonequilibrium stage of the experimental result, the axial strain-stress curves of the sample with different initial densities could be obtained (Figure 8(a)). The stress-strain curves shift upwards with the increase of initial mass density. The unloading curve shows an initial steep reduction in stress without recovery of deformation, followed by a further reduction in stress with a slight recovery of deformation.

The rigid confined compression test is oedometric, and the e-lop σ curve is usually used to describe the deformation of the sample, where e is the void ratio of the sample and σ is the axial stress on the sample. In a one-dimensional

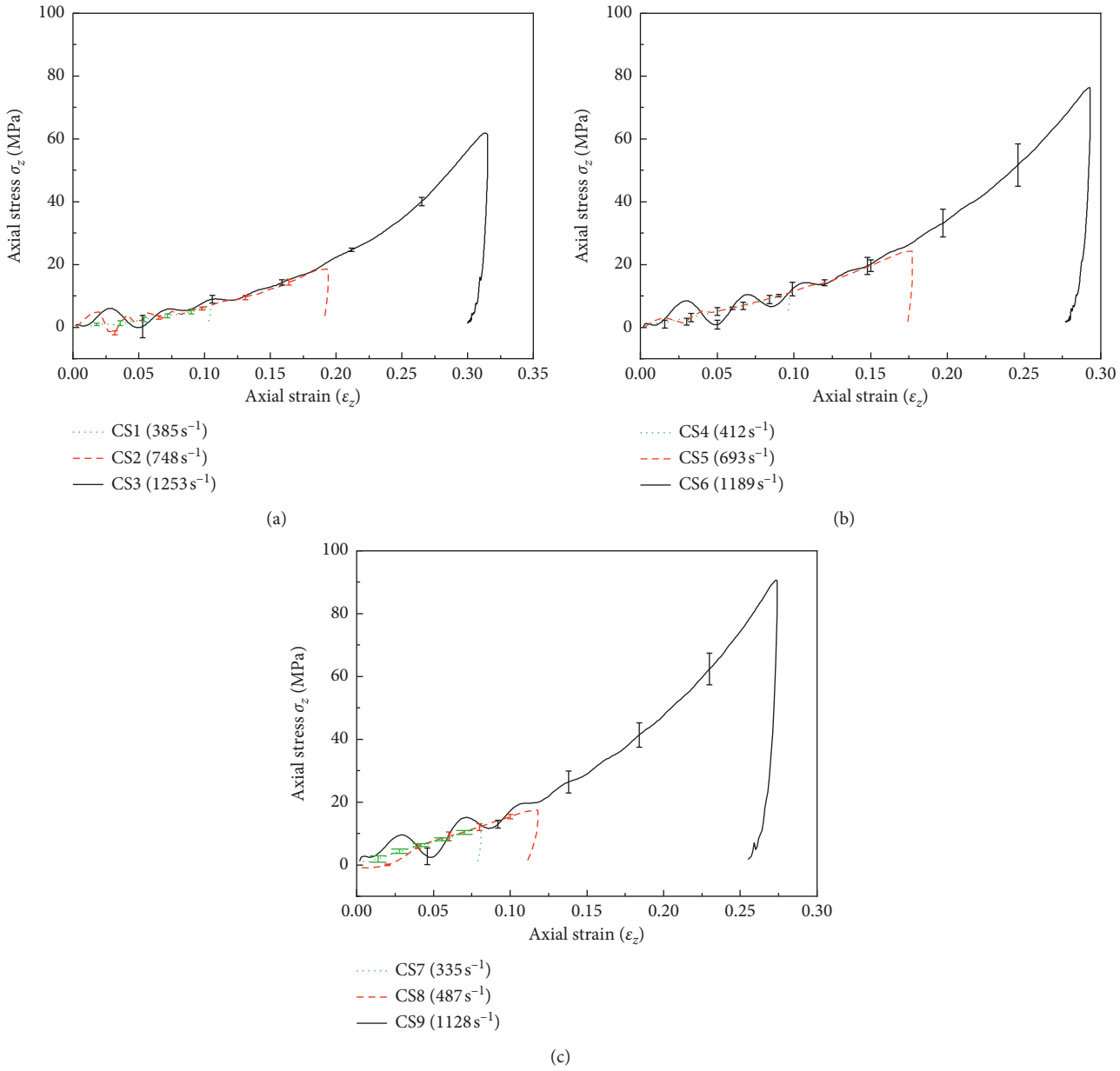

FIGURE 7: Effect of strain rate on the dynamic axial response of calcareous sand. The average axial strain-stress curves of calcareous sand with initial densities of (a) 1.26 g/cm^3, (b) 1.35 g/cm^3, and (c) 1.42 g/cm^3.

compression test, the lateral strain is approximately zero when compared with the axial strain, so the void ratio is given by

$$e = \frac{G_S}{\rho} - 1, \qquad \rho = \frac{\rho_0}{(1 - \varepsilon_z)}, \tag{2}$$

where ρ and ρ_0 are the current and initial densities of the sample, respectively; G_s is the density of the soil particle; and ε_z is the axial strain.

According to equation (2), the axial strain-strain experimental results shown in Figure 8(a) could be transferred into e-log σ curves (Figure 8(b)). As the sand particles are crushable, the initial skeleton of calcareous sand is unstable under high stresses. With increasing stress, the initial skeleton structure of the calcareous sand was gradually destroyed and a stable structure formed. So at a certain stress, the e-log σ curve is independent of the initial sample skeleton properties and the initial density of the sample. So, all the loading curves of calcareous sands with different initial densities in Figure 8(b) merge into a same straight line at an axial stress of about 40 MPa. The slope of the line is the compression index and is 0.239 for this calcareous sand under dynamic compression. Luo et al. studied the dynamic compression behaviour of quartz sand, and the compression

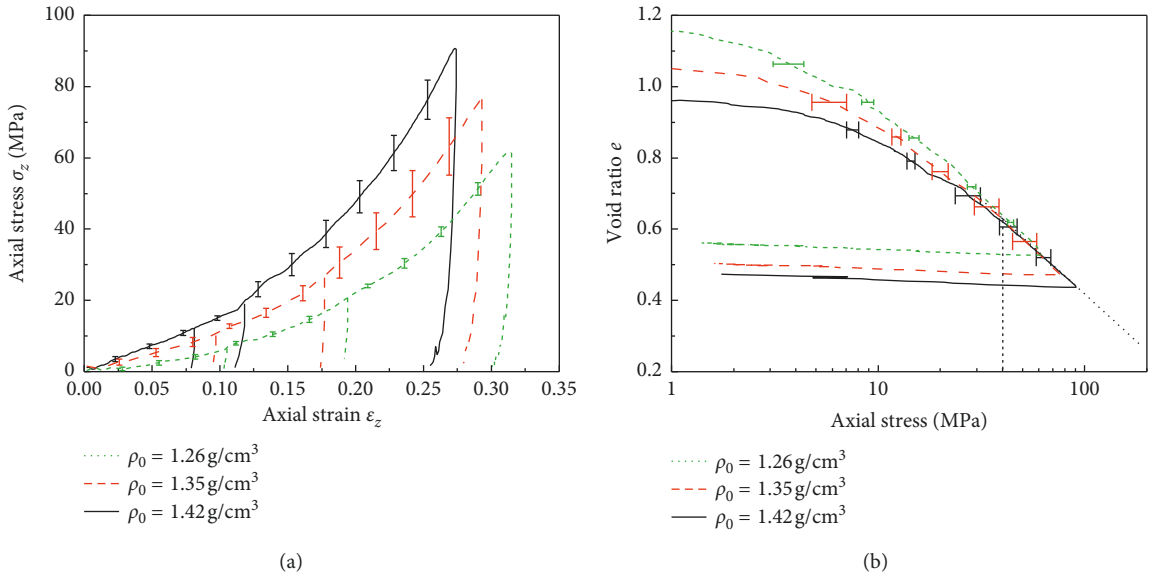

Figure 8: Effect of initial density on the dynamic axial response of calcareous sand. (a) The axial strain-stress curves of calcareous sand. (b) The e-log σ curves of calcareous sand.

index is 0.281 to 0.312 [15], indicating the calcareous sand is "softer" than quartz sand.

3.2. Deviatoric and Volumetric Behaviours of the Sand. For the sand sample confined by the sleeve within the elastic range, the lateral stress σ_r is given by

$$\sigma_r = \frac{1}{2\kappa}\left[\left(\frac{r_o}{r_i}\right)^2 - 1\right]E_s\varepsilon_\theta, \tag{3}$$

where r_o and r_i represent the outer and inner radii of the sleeve; E_s is Young's modulus of the sleeve; ε_θ is the circumferential strain on the sleeve; and κ is a correction coefficient for the effect of the smaller sample length compared with that of the sleeve, which could be derived from the numerical method [29, 30].

Here, the correction coefficient is given by equation (4), which is obtained by numerical analysis [30], where l is the current thickness of the sample:

$$\kappa = 0.0598l + 0.0162. \tag{4}$$

Figure 9 shows the axial stress and lateral stress histories of calcareous sand in test group CS9. The lateral stress coefficient k_0 is defined as

$$k_0 = \frac{\sigma_r}{\sigma_z}, \tag{5}$$

where σ_r is the lateral stress and σ_z is maximum the axial stress. To improve the precision of k_0, it could be calculated using equation (5) by using the maximum values of the stresses. The mean experimental results of k_0 in different test groups and corresponding error bars are summarised in

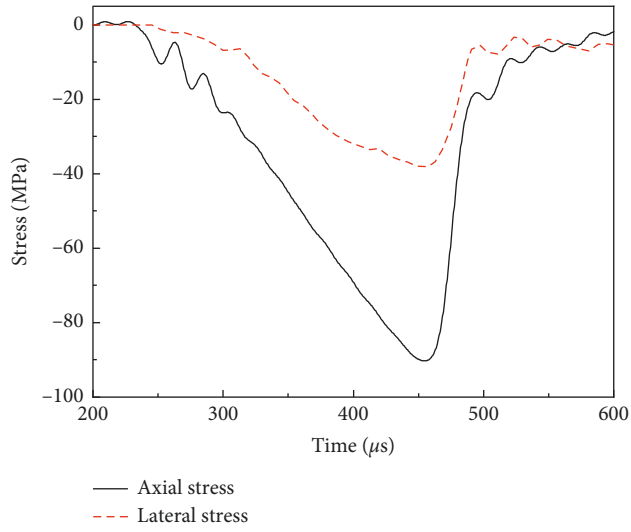

Figure 9: Typical axial stress and lateral stress histories of calcareous sand (test group number: CS9).

Figure 10. The results show that the lateral stress coefficient increases as the axial stress increases.

In a confined SHPB experiment, the hydrostatic pressure (isotropic stress) component p and equivalent von Mises stress σ_Y are given by [15]

$$p = \frac{1}{3}(\sigma_z + 2\sigma_r),$$
$$\sigma_Y = \sigma_z - \sigma_r. \tag{6}$$

Based on equation (5), the aforementioned equations could be transformed to give

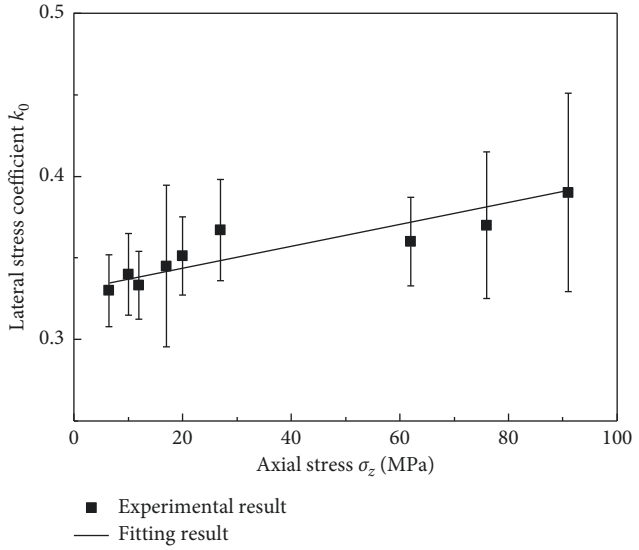

Figure 10: Relationship between lateral stress coefficient and axial stress.

$$p = \frac{1 + 2k_0}{3}\sigma_z,$$
$$\sigma_Y = (1 - k_0)\sigma_z. \tag{7}$$

The Drucker–Prager yield function is usually used to describe the deviatoric behaviour of soils under low pressure, in which the von Mises stress is linearly dependent on hydrostatic pressure. Based on this yield function, the lateral stress coefficient is shown to be a constant according to equation (7), which is inconsistent with the experimental results from tests on calcareous sand. To describe why k_0 increases as the axial stress increases, the Lundborg model is used to describe the deviatoric behaviour of calcareous sand, whose yield function is expressed as [31]

$$\sigma_Y = \frac{\mu p}{1 + \left(\mu p / \sigma_{Y_{\max}}\right)}, \tag{8}$$

where μ and $\sigma_{Y\max}$ are the material constants. Substituting equation (7) into the above equation, the relationship between lateral stress coefficient and axial stress is given by

$$\sigma_z = \frac{(2\mu + 3)k_0 + (\mu - 3)}{\mu(1 - k_0)(1 + 2k_0)}\sigma_{Y_{\max}}. \tag{9}$$

The material constants μ and $\sigma_{Y\max}$ could be obtained by fitting the experimental results from equation (9), and the corresponding results are $\mu = 1.21$ and $\sigma_{Y\max} = 363$ MPa. The fitting curve is shown in Figure 10, and the yield function is shown in Figure 11.

Based on the axial strain-stress experimental results (Figure 8(a)), the volumetric behaviour of dry calcareous sand in the form of density-pressure relationship could be obtained by using equations (2), (7), and (9), and the results are shown in Figure 12. To describe how the slope of the curves increases as the pressure increases, the Murnaghan

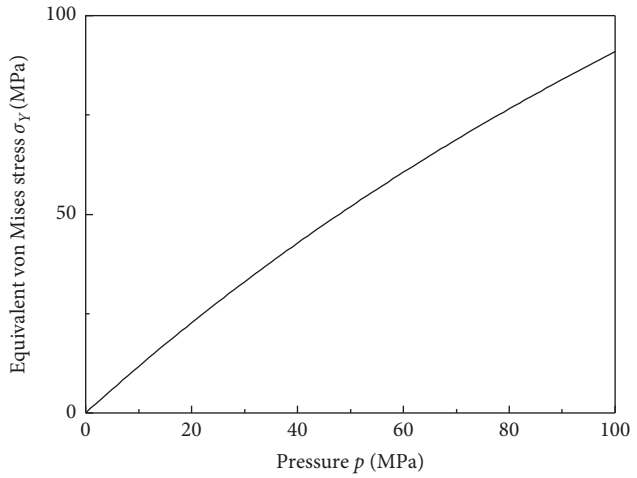

Figure 11: Lundborg yield surface of the calcareous sand.

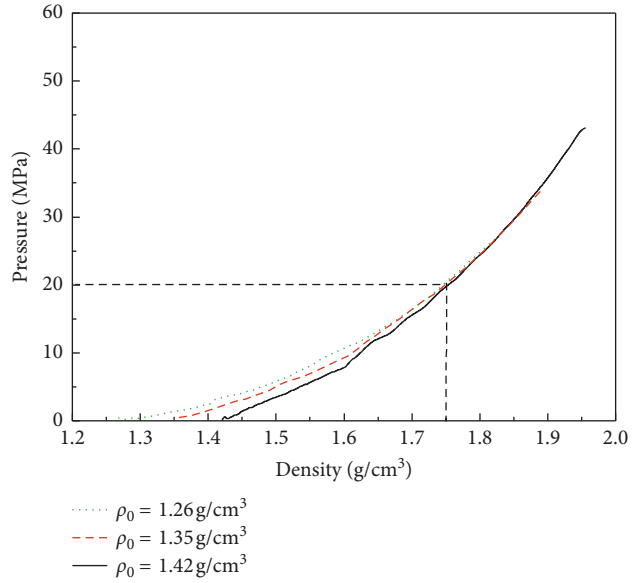

Figure 12: Effect of initial density on the density-pressure relationship of dry calcareous sand.

equation [32, 33] was used to model the volumetric behaviour of dry calcareous sand:

$$p = \frac{k}{n_k}\left[\left(\frac{\rho}{\rho_0}\right)^{n_k} - 1\right], \tag{10}$$

where k and n_k are the material constants, which could be obtained by fitting the equation with experimental data.

The experimental results shown in Figure 12 show that the density-pressure curves of samples with different initial densities could be separated into two segments at the point where the density is 1.75 g/cm^3. In the first segment, the curves are dependent on the initial density of the sample, whereas in the second segment, the curves are independent of the initial density of the sample; therefore, the curves should be fitted separately.

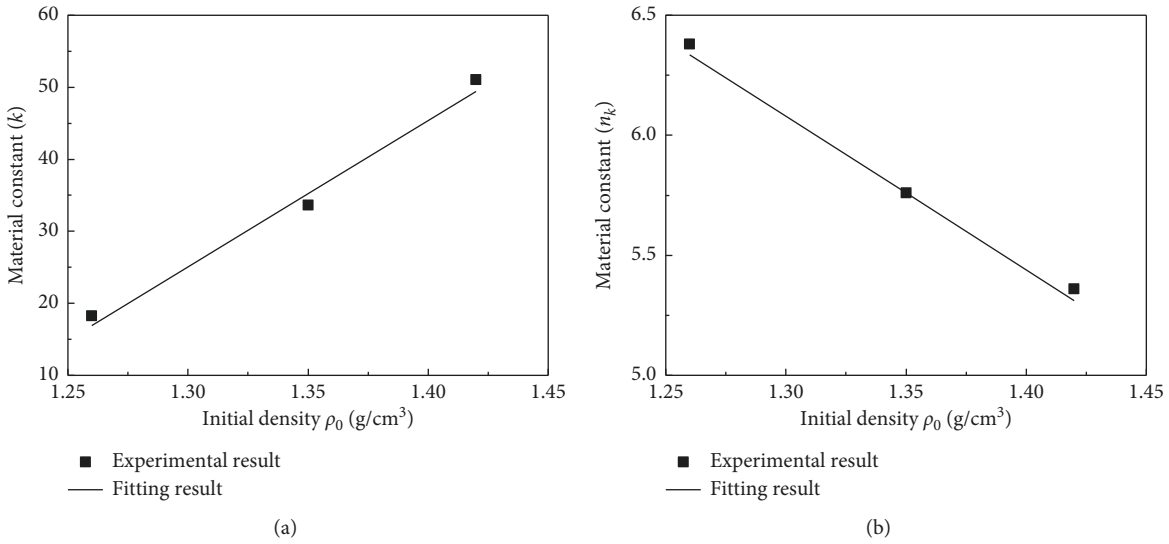

Figure 13: Relationship between material constants and initial density of the sample. (a) Material constant k. (b) Material constant n_k.

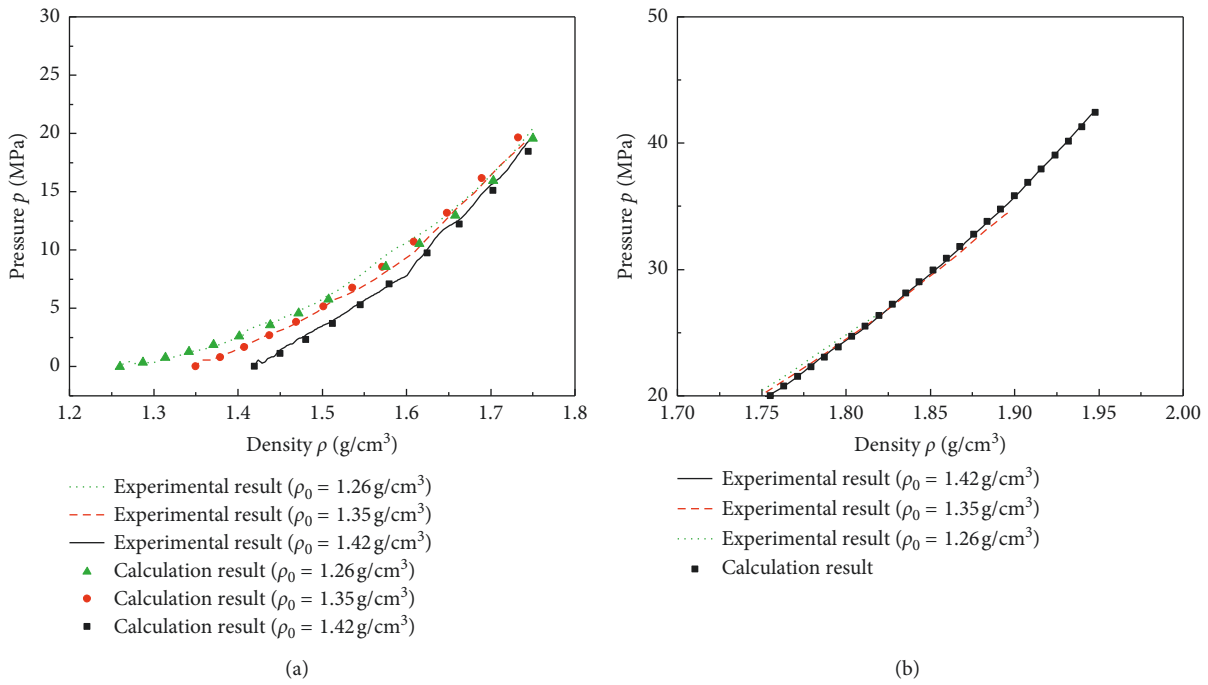

Figure 14: Comparison between experimental and calculated results. Comparison of (a) the first segment and (b) the second segment.

For the first segment, the relationships between the material constants using data fitted to equation (10) with the initial sample density are summarised in Figures 13(a) and 13(b). The results show that the material constants are related to the initial density of the sample in a quasilinear manner as follows:

$$k = 203.2\rho_0 - 239.1,$$
$$n_k = 14.4 - 6.4\rho_0. \quad (11)$$

The second segment of the density-pressure curve is independent of the sample initial density, so ρ_0 in equation (10) could be chosen as 1.42 g/cm^3. The corresponding material parameter fitting results are $n_k = 5.46$ and $k = 50.1$.

In summary, the density-pressure relationship of dry calcareous sand with any initial density ρ_0 could be summarised as

$$p = \begin{cases} \dfrac{k}{n_k}\left[\left(\dfrac{\rho}{\rho_0}\right)^{n_k} - 1\right], & \rho \le 1.75\ \text{g/cm}^3, \\ \dfrac{50.1}{5.46}\left[\left(\dfrac{\rho}{1.42}\right)^{5.46} - 1\right], & \rho > 1.75\ \text{g/cm}^3, \end{cases} \tag{12}$$

where the material constants k and n_k could be calculated by using equation (11) and the comparison between experimental results and those arising from the use of equation (12) is shown in Figure 14. By comparing the calculation results and the test results shown in the figure, it can be seen that equation (12) could well describe the dynamic volumetric behaviour of dry calcareous sand.

4. Conclusions

The dynamic mechanical behaviour of dry calcareous sand under rigid confinement provided by a thick-wall stainless steel sleeve was investigated using a split Hopkinson pressure bar (SHPB) at high strain rates ($335\ \text{s}^{-1}$ to $1253\ \text{s}^{-1}$). A new sand specimen assembly by using Glyd Ring was developed, and the assembly relies on repeated dynamic compaction to prepare sand samples with precise initial mass densities. Sand samples with three initial mass densities ($1.26\ \text{g/cm}^3$, $1.35\ \text{g/cm}^3$, and $1.42\ \text{g/cm}^3$) were compressed at three nominal striker velocities (5 m/s, 10 m/s, and 20 m/s). A strain gauge was attached to the external surface of the sleeve to measure the circumferential strain therein, and hence, the deviatoric and volumetric behaviours of calcareous sand could be determined.

Experimental results show that, in the strain rate range of $335\ \text{s}^{-1}$ to $1253\ \text{s}^{-1}$, the dynamic compression characteristics of dry calcareous sand exhibited no significant rate effect. The e-log σ curves of samples with different initial densities merge into one straight line whose slope is 0.239 at an axial stress of 40 MPa. The dynamic compression index of dry calcareous sand is much smaller than that of quartz sand, indicating that the dry calcareous sand is much "softer." The lateral stress coefficient of calcareous sand increases with axial stress, so the Lundborg model could be used to describe its deviatoric behaviour. The density-pressure curves of dry calcareous sand could be separated into two segments when the density is $1.75\ \text{g/cm}^3$; in the first segment, the curve is dependent on the initial density, whereas in the second segment, it is independent thereof. In both segments, the curve could be described by the Murnaghan equation.

Data Availability

The data used to support the findings of this study are available from the corresponding author upon request.

Conflicts of Interest

The authors declare that there are no conflicts of interest regarding the publication of this paper.

Acknowledgments

The financial support was provided by the National Natural Foundation for Young Scientists of China (Grant no. 51409257).

References

[1] M. Datta, G. V. Rao, and S. K. Gulhati, "The nature and engineering behavior of carbonate soils at Bombay high, India," *Marine Geotechnology*, vol. 4, no. 4, pp. 307–341, 1981.

[2] B. Sterianos, *Geotechnical properties of carbonate soils with reference to an improved engineering classification*, Ph.D. thesis, University of Cape Town, Cape Town, South Africa, 1988.

[3] J. L. Alba and J. M. Audibert, "Pile design in calcareous and carbonaceous granular materials, and historic review," in *Proceedings of the 2nd International Conference on Engineering for Calcareous Sediments*, vol. 1, pp. 29–44, AA Balkema, Bahrain, February 1999.

[4] X.-Z. Wang, Y.-Y. Jiao, R. Wang, M.-J. Hu, Q.-S. Meng, and F.-Y. Tan, "Engineering characteristics of the calcareous sand in Nansha Islands, South China Sea," *Engineering Geology*, vol. 120, no. 1–4, pp. 40–47, 2011.

[5] F. A. Chuhan, A. Kjeldstad, K. Bjørlykke, and K. Høeg, "Experimental compression of loose sands: relevance to porosity reduction during burial in sedimentary basins," *Canadian Geotechnical Journal*, vol. 40, no. 5, pp. 995–1011, 2003.

[6] M. R. Coop, "The behaviour of granular soils at elevated stresses," *Predictive Soil Mechanics: Proceedings of the Wroth Memorial Symposium*, pp. 186–198, Oxford, UK, July 1993.

[7] M. R. Coop, "The mechanics of uncemented carbonate sands," *Géotechnique*, vol. 40, no. 4, pp. 607–626, 1990.

[8] Y. Nakata, M. Hyodo, A. F. L. Hyde, Y. Kato, and H. Murata, "Microscopic particle crushing of sand subjected to high pressure one-dimensional compression," *Soils and Foundations*, vol. 41, no. 1, pp. 69–82, 2001.

[9] J. V. Farr, *Loading Rate Effects on the One-Dimensional Compressibility of Four Partially Saturated Soils*, Army Engineer Waterways Experiment Station Vicksburg Ms Structures Lab, Vicksburg, MS, USA, 1986.

[10] C. W. Felice, *The response of soil to impulse loads using the split-Hopkinson pressure bar technique*, Ph.D. thesis, The University of Utah, Salt Lake City, UT, USA, 1986.

[11] A. M. Bragov, V. L. Kotov, A. K. Lomunov, and I. V. Sergeichev, "Measurement of the dynamic characteristics of soft soils using the kolsky method," *Journal of Applied Mechanics and Technical Physics*, vol. 45, no. 4, pp. 580–585, 2004.

[12] J. Semblat, M. P. Luong, and G. Gary, "3D-Hopkinson bar: new experiments for dynamic testing on soils," *Soils and Foundations*, vol. 39, no. 1, pp. 1–10, 1999.

[13] B. E. Martin, W. Chen, B. Song, and S. A. Akers, "Moisture effects on the high strain-rate behavior of sand," *Mechanics of Materials*, vol. 41, no. 6, pp. 786–798, 2009.

[14] B. Song, W. Chen, and V. Luk, "Impact compressive response of dry sand," *Mechanics of Materials*, vol. 41, no. 6, pp. 777–785, 2009.

[15] H. Luo, H. Lu, W. L. Cooper, and R. Komanduri, "Effect of mass density on the compressive behavior of dry sand under confinement at high strain rates," *Experimental Mechanics*, vol. 51, no. 9, pp. 1499–1510, 2011.

[16] H. Lu, H. Luo, and R. Komaduri, "Dynamic compressive response of sand under confinements," in *Proceedings of the SEM Annual Conference*, Society of Experimental Mechanics Inc., Bethel, CT, USA, 2009.
[17] J. Huang, S. Xu, and S. Hu, "Effects of grain size and gradation on the dynamic responses of quartz sands," *International Journal of Impact Engineering*, vol. 59, pp. 1–10, 2013.
[18] A. D. Barr, *Strain-rate effects in quartz sand*, Ph.D. thesis, University of Sheffield, Sheffield, UK, 2016.
[19] Y. Lv, J. Liu, and Z. Xiong, "One-dimensional dynamic compressive behavior of dry calcareous sand at high strain rates," *Journal of Rock Mechanics and Geotechnical Engineering*, vol. 11, no. 1, pp. 196–205, 2019.
[20] ASTM D854, *Standard Test Methods for Specific Gravity of Soil Solids by Water Pycnometer*, ASTM, West Conshohocken, PA, USA, 2010.
[21] ASTM D4253, *Standard Test Methods for Maximum Index Density and Unit Weight of Soils Using a Vibratory Table*, ASTM, West Conshohocken, PA, USA, 2006.
[22] ASTM D4254, *Standard Test Methods for Minimum Index Density and Unit Weight of Soils and Calculation of Relative Density*, ASTM, West Conshohocken, PA, USA, 2006.
[23] G. Kolsky, "Mechanical characteristics of materials at high loading rates," *Mekhanika*, vol. 4, pp. 108–119, 1950.
[24] W. W. Chen and B. Song, *Split Hopkinson (Kolsky) Bar: Design, Testing and Applications*, Springer Science & Business Media, Berlin, Germany, 2010.
[25] K. Ravi-Chandar and Z. Ma, "Inelastic deformation in polymers under multiaxial compression," *Mechanics of Time-Dependent Materials*, vol. 4, no. 4, pp. 333–357, 2000.
[26] M.-N. Bussac, P. Collet, G. Gary, and R. Othman, "An optimisation method for separating and rebuilding one-dimensional dispersive waves from multi-point measurements. Application to elastic or viscoelastic bars," *Journal of the Mechanics and Physics of Solids*, vol. 50, no. 2, pp. 321–349, 2002.
[27] A. Tyas and D. J. Pope, "Full correction of first-mode Pochammer–Chree dispersion effects in experimental pressure bar signals," *Measurement Science and Technology*, vol. 16, no. 3, pp. 642–652, 2005.
[28] A. Tyas and A. J. Watson, "An investigation of frequency domain dispersion correction of pressure bar signals," *International Journal of Impact Engineering*, vol. 25, no. 1, pp. 87–101, 2001.
[29] J. A. Yamamuro, P. A. Bopp, and P. V. Lade, "One-dimensional compression of sands at high pressures," *Journal of Geotechnical Engineering*, vol. 122, no. 2, pp. 147–154, 1996.
[30] Z. Wen, Y. Qiu, Z. Min, Z. Zhao, and M. Wang, "Experimental study on quasi-one-dimensional strain compression of calcareous sand," *Explosion and Shock Waves*, vol. 2019, pp. 1–11, 2019.
[31] N. Lundborg, "Strength of rock-like materials," *International Journal of Rock Mechanics and Mining Sciences & Geomechanics Abstracts*, vol. 5, no. 5, pp. 427–454, 1968.
[32] F. D. Murnaghan, "The compressibility of media under extreme pressures," *Proceedings of the National Academy of Sciences*, vol. 30, no. 9, pp. 244–247, 1944.
[33] D. H. Chung, H. Wang, and G. Simmons, "On the calculation of the seismic parameter ϕ at high pressure and high temperatures," *Journal of Geophysical Research*, vol. 75, no. 26, pp. 5113–5120, 1970.